optica

Photon-sparse microscopy: visible light imaging using infrared illumination

Reuben S. Aspden,[1] Nathan R. Gemmell,[2] Peter A. Morris,[1] Daniel S. Tasca,[1,7] Lena Mertens,[1] Michael G. Tanner,[3,8] Robert A. Kirkwood,[3] Alessandro Ruggeri,[4] Alberto Tosi,[4] Robert W. Boyd,[5,6] Gerald S. Buller,[2] Robert H. Hadfield,[3] and Miles J. Padgett[1,*]

[1]SUPA, School of Physics and Astronomy, University of Glasgow, Glasgow, G12 8QQ, UK
[2]SUPA, School of Engineering & Physical Sciences, Heriot-Watt University, Edinburgh, EH14 4AS, UK
[3]SUPA, School of Engineering, University of Glasgow, Glasgow, G12 8QQ, UK
[4]Dipartimento di Elettronica, Informazione e Bioingegneria Politecnico di Milano, Piazza Leonardo da Vinci 32, 20133 Milano, Italy
[5]Department of Physics, University of Ottawa, Ottawa, Ontario, Canada
[6]The Institute of Optics and Department of Physics and Astronomy, University of Rochester, Rochester, New York 14627, USA
[7]Current address: Instituto de Física, Universidade Federal do Rio de Janeiro, Caixa-Postal 68528, Rio de Janeiro, RJ 21941-972, Brazil
[8]Current address: SUPA, School of Engineering & Physical Sciences, Heriot-Watt University, Edinburgh, EH14 4AS, UK
*Corresponding author: miles.padgett@glasgow.ac.uk

Received 26 June 2015; revised 15 October 2015; accepted 29 October 2015 (Doc. ID 243868); published 10 December 2015

Conventional imaging systems rely upon illumination light that is scattered or transmitted by the object and subsequently imaged. Ghost-imaging systems based on parametric down-conversion use twin beams of position-correlated signal and idler photons. One beam illuminates an object while the image information is recovered from a second beam that has never interacted with the object. In this Letter, we report on a camera-based ghost imaging system where the correlated photons have significantly different wavelengths. Infrared photons at 1550 nm wavelength illuminate the object and are detected by an InGaAs/InP single-photon avalanche diode. The image data are recorded from the coincidently detected, position-correlated, visible photons at a wavelength of 460 nm using a highly efficient, low-noise, photon-counting camera. The efficient transfer of the image information from infrared illumination to visible detection wavelengths and the ability to count single photons allows the acquisition of an image while illuminating the object with an optical power density of only 100 pJ cm^{-2} s^{-1}. This wavelength-transforming ghost-imaging technique has potential for the imaging of light-sensitive specimens or where covert operation is desired. © 2015 Optical Society of America

OCIS codes: (110.0180) Microscopy; (110.3080) Infrared imaging; (230.7405) Wavelength conversion devices.

http://dx.doi.org/10.1364/OPTICA.2.001049

Low-light-level imaging at infrared wavelengths has many applications within both the technological and biological sectors. These applications span covert security systems, the imaging of light-sensitive biological samples, and imaging within semiconductor devices. However, given that the majority of single-photon-sensitive, large-format detector arrays are silicon-based and therefore ineffective at wavelengths greater than 1 μm, the technological difficulties with such applications are readily apparent: crafting a camera with high quantum efficiency and low noise at infrared wavelengths is difficult and expensive.

In this Letter, we circumvent the lack of infrared cameras that combine low-noise with single-photon sensitivity by performing the imaging using the so-called "ghost imaging" method. This method utilizes the spatial correlations between photons in the two output beams, signal and idler, generated through the spontaneous parametric down-conversion (SPDC) process [1].

In the 1990s, it was shown how the correlations between photons generated through SPDC could be utilized to create imaging systems [2,3]. These ghost-imaging systems rely on the strong position correlations between the beams of signal and idler photons that are produced by the SPDC process [4]. In a ghost-imaging system a transmissive object is placed in the idler beam and the transmitted photons are measured using a single-element, heralding detector. The use of a single-element detector means that measurements of photons that probe the object reveal no spatial information. In parallel to these measurements of the idler photons, a scanning single-element detector measures the corresponding signal photons—but since these signal photons do not interact with the object, again no image is formed. However, although the data from either detector on its own does not reveal an image, the correlation between the two data sets gives an image of the object. It should be noted that while ghost imaging based on parametric down-conversion is not reliant on quantum entanglement, the implicit entanglement within down-conversion provides a simple and practical source of spatially correlated photons. It has also been shown that a form of ghost imaging is possible with classical light [4–6], albeit using higher light levels where classical correlations persist even in the presence of shot noise. However, ghost imaging based on parametric down-conversion uses correlations

between individual photon pairs, and hence has unique attributes in ultra-low-light imaging. With one exception [7], in all ghost-imaging systems based on parametric down-conversion, the signal and idler have the same (degenerate) or similar wavelengths [8–10].

From a practical point of view, forming an image with light that does not directly interact with the object sounds useful. However, although the signal photons striking the position-sensitive detector have never interacted with the object, the object is still subject to illumination by an equivalent number of idler photons. Until recently, all systems based on photon pairs implemented their position-recording detector by raster-scanning a single-element detector. This reliance upon scanning meant that the maximum optical efficiency of such systems could not exceed 1/N, where N is the number of pixels in the image. We overcame this limitation by using a time-gated camera that could detect the position of a single photon across the full field of view of an imaging system [11,12]. However, in that work, both the signal and idler beams had the same wavelength, and hence the system did not have the wavelength-transforming capability of this present work. The present system combines the increased detection efficiency offered by a time-gated camera with the wavelength-transforming advantages of nondegenerate ghost-imaging techniques. This combination enables ultra-low illumination infrared imaging of microscopic objects using signal and idler photons with a wavelength ratio of 1:3.

High-contrast microscopy using infrared illumination has previously been achieved using structured illumination or masking and a single-pixel detector [13,14]. However, these techniques rely on measuring a small change in signal on a large background light level, and therefore require far higher illumination powers than the single-photon regime utilized in the present work. Another technique used to image with infrared illumination is wavelength upconversion. In this technique, infrared photons illuminate the object and are then converted to a visible wavelength before being detected. However, this upconversion process suffers either degraded resolution or low conversion efficiency [15–17]. In 2014, an ingenious approach to transforming wavelength between the illumination and recording light was demonstrated by Lemos *et al.* [18]. Perhaps the most exciting aspect of that experiment was the ability to form an image without an infrared detector of any type. However, the photon flux in that imaging system was maintained at a modest level so that the image was detectable above the noise floor of a conventional low-light camera.

In this Letter, we implement a camera-based, ghost-imaging approach but use signal and idler photons at dramatically different wavelengths. Infrared photons at 1550 nm wavelength illuminate/probe the object, yet the camera data is recorded from visible photons at 460 nm that are correlated in position with the infrared photons. This configuration allows for the irradiation of the object with low-energy, infrared photons while still making use of a visible-wavelength, highly sensitive camera. The single-photon sensitivity and high timing resolution of both the heralding detector and the imaging camera allows for the use of an extremely low illumination flux, of order $\sim 10^5$ infrared photons impinging on the object per second.

A schematic of our imaging system, shown in Fig. 1, utilizes the photon pairs generated through a highly nondegenerate SPDC process giving signal and idler wavelengths of 460 and 1550 nm, respectively. The signal and idler photons are separated

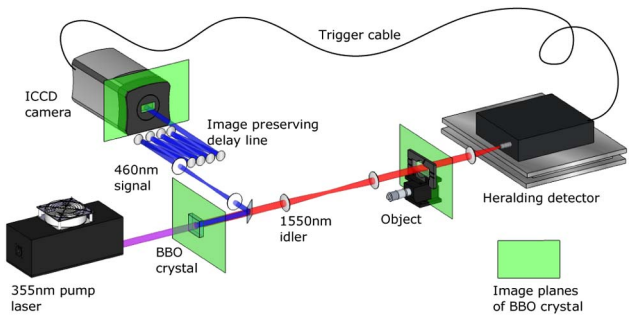

Fig. 1. Experimental setup. The nondegenerate SPDC process generates a visible/infrared photon pair at the BBO crystal, and these photons are split at a dichroic mirror. The infrared photon probes an object and the transmitted photons are detected by a single-element heralding detector (InGaAs/InP single-photon avalanche diode). This detection event triggers the intensifier of the ICCD camera, which detects the delayed yet spatially correlated visible photon. The recovered image of the object is the accumulation of many visible photon detections by the ICCD.

at a dichroic mirror and directed along different optical paths. The idler path contains an object that is placed in an image plane of the SPDC crystal. The idler photons that are transmitted through the object are then detected by a single-element, free-space coupled InGaAs/InP single-photon avalanche diode (SPAD) [19]. We refer to this detector as the heralding detector. In the signal path, the plane of the crystal is reimaged to a time-gated, intensified camera with a CCD detector array (ICCD). The effective magnification of our system from object plane to ICCD is $M = 10$ (see Supplement 1). The detection of an infrared probe photon by the heralding detector is used to trigger the gate of the intensifier in the ICCD such that the signal photon that is imaged is the position-correlated visible twin of the idler photon. To ensure that we image only the correlated signal photon, we compensate for the electronic delay associated with the SPAD and the intensifier in the ICCD by a free-space, image-preserving delay line within the signal path (see Supplement 1). The average power (typically 50 mW) and repetition rate of the pump laser (100 MHz), coupled with the gating time of the intensifier (10 ns) produces a down-conversion flux such that the camera typically detects no more than one photon per triggering of the intensifier. Typically the trigger rate of the intensifier is ~ 10 kHz and the exposure time (i.e., integration time) of the camera is 0.1 s, meaning that the intensifier is triggered many times per camera frame. Each triggering of the camera should, in principle, yield a measured photon. However, in practice, this efficiency is set by the optical throughput of the signal path and the quantum efficiency of the ICCD camera to approximately 7%. Although giving 50–100 photons per frame, the large number of camera pixels means there is on average much less than one photon per pixel in each frame. To each frame, we then apply our photon-counting methodology (see Supplement 1) to convert these frames into photons per pixel. We then sum the photons detected over many frames to give an accumulated image. The resulting image data is again in the form of number of detected photons per pixel. The computational overhead of data transfer means that at a frame exposure time of 0.1 s, we can acquire six frames per second.

To illustrate the wavelength-transforming capabilities of our system, we use an object formed from a polished silicon wafer onto which was patterned a microscopic gold test target

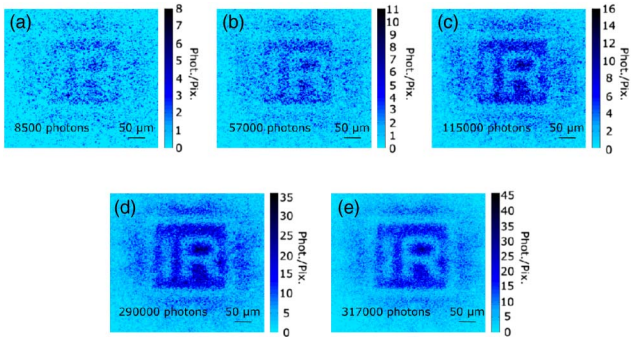

Fig. 2. Image of a test object. A stencil of the letter "IR" obtained in visible light by an ICCD camera, even though the object was illuminated only by infrared radiation. The object is etched into gold deposited onto a 387 μm thick silicon substrate. For every infrared photon that probed the object and was detected by the heralding detector, the ICCD camera was triggered to record the position-correlated visible photon. The images were formed by summing over many photon-detection events as labeled.

(created by electron beam lithography, electron beam deposition, and liftoff). The height of the letters ("IR") to be imaged are 120 μm, set within a framing box of width 160 μm. At a wavelength of 1550 nm, the silicon is transparent whereas the gold layer is not. Note that any residual 460 nm signal photons that are in the idler path will be fully absorbed by the silicon substrate and therefore cannot trigger the heralding detector. We also note that any 1550 nm photons in the signal path will not be detectable by the ICCD camera, as the photons are outside the spectral range of the photocathode of the intensifier.

Figure 2 shows images corresponding to the accumulation of photons as more of the ICCD camera frames are summed together to recover the accumulated images. In this case, the duration of data acquisition ranged from 30 s to 10 min. Even with extremely photon-sparse images, it is possible to use reconstruction techniques to recover images of high visual quality [12] (see Supplement 1).

Two useful figures of merit for measuring the quality of an imaging system are the resolution and the contrast of the acquired images. In Fig. 3, we show long exposure images of a silicon "λ" on a gold background and a gold "IR" on a silicon background. The images were acquired using the settings just detailed and a 30 min total exposure time, yielding an image contrast of 71%. The spatial resolution of the system corresponds to a point spread function of approximately 15 μm (2σ). This spatial resolution is fundamentally limited by a combination of the strength of the spatial correlation between the down-converted signal and idler photons and the diffraction limit of the various relay optics,

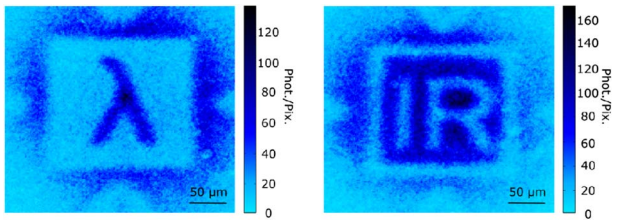

Fig. 3. Silicon "λ" on a gold background and a gold "IR" on a silicon background. These visible images produced from the infrared illumination correspond to a total accumulation time of 30 min.

(see Supplement 1). Our understanding is that this in no way exceeds the classical limit.

The images in Fig. 2 were acquired by detection of between 8500 photons in image (a) and 317,000 photons in image (e). However, when considering low-light imaging, the number of photons detected by the camera is not the most pressing consideration. Rather, the most important characteristic is the number of photons incident on the object for the duration of the acquisition. We calculate this by measuring the number of photons detected by the heralding detector with no object present. Given the detection efficiency of this heralding detector, we can infer the number of infrared photons at the plane of the object within the boundary box of the object to be 2×10^5 photons per second. This photon flux corresponds to an illumination power of 25 fW, and an energy deposition on the object of approximately 100 pJ cm^{-2} s^{-1}. Figures 2(a) and 2(e) were acquired for a total exposure time of 30 s and 10 min, respectively, and thus the total energy deposition on the object within the boundary box was 750 fJ and 15 pJ, respectively. There is an obvious tradeoff between a long exposure time resulting in high image quality and a shorter exposure time with lower energy deposition but resulting in lower-quality images.

Imaging a silicon/gold object, while not being photosensitive itself, demonstrates the low-light imaging capabilities of our system. The conditional nature of our detection scheme, which depends upon the correlated detection of IR and visible photons, reduces our overall quantum efficiency to the order of 7%, which compares to a quantum efficiency of a leading shortwave infrared low-light camera of 85%. In terms of dark noise, we measure our detection scheme to have a measured dark noise rate of 0.01 noise events per pixel per second, compared with eight noise events per pixel per second from leading shortwave infrared (1.5 μm) low-light cameras [20]. Taking these factors together, we are able to image with higher contrast using a lower illumination power without losing the image in the noise floor of the camera.

In conclusion, we have demonstrated that it is possible to obtain microscope images from visible photons at 460 nm by illuminating the object with an equal number of position-correlated infrared photons at 1550 nm. To the best of our knowledge, this is the first time ghost imaging has been performed with such a large ratio between signal and idler wavelength, and certainly the first time that this has been combined with an array-type detector. The ability to translate the image information from infrared to visible wavelengths has potential for imaging light-sensitive specimens or where covert operation is desired [21].

Funding. Engineering and Physical Sciences Research Council (EPSRC) (EP/I012451/1, K015338/1); European Research Council (ERC) (192382).

Acknowledgment. RAK and RHH gratefully acknowledge the staff of the James Watt Nanofabrication Centre at GU for expert support in preparing the imaging test object. RWB acknowledges support by the Canada Excellence Research Chair Program and from the US Defense Threat Reduction Agency.

See Supplement 1 for supporting content.

REFERENCES AND NOTE

1. S. P. Walborn, C. H. Monken, S. Pádua, and P. H. Souto Ribeiro, Phys. Rep. **495**, 87 (2010).

2. T. B. Pittman, Y. H. Shih, D. V. Strekalov, and A. V. Sergienko, Phys. Rev. A **52**, R3429 (1995).
3. C. H. Monken, P. H. S. Ribeiro, and S. Pádua, Phys. Rev. A **57**, 3123 (1998).
4. J. H. Shapiro and R. W. Boyd, Quantum Inf. Process. **11**, 949 (2012).
5. R. S. Bennink, S. J. Bentley, and R. W. Boyd, Phys. Rev. Lett. **89**, 113601 (2002).
6. A. Gatti, E. Brambilla, M. Bache, and L. A. Lugiato, Phys. Rev. Lett. **93**, 093602 (2004).
7. C. C. Kim and G. Kanner, Proc. SPIE **7815**, 781503 (2010).
8. J. C. Howell, R. S. Bennink, S. J. Bentley, and R. W. Boyd, Phys. Rev. Lett. **92**, 210403 (2004).
9. S. Karmakar and Y. Shih, Phys. Rev. A **81**, 033845 (2010).
10. O. S. Magaña-Loaiza, G. A. Howland, M. Malik, J. C. Howell, and R. W. Boyd, Appl. Phys. Lett. **102**, 231104 (2013).
11. R. S. Aspden, D. S. Tasca, R. W. Boyd, and M. J. Padgett, New J. Phys. **15**, 073032 (2013).
12. P. A. Morris, R. S. Aspden, J. E. C. Bell, R. W. Boyd, and M. J. Padgett, Nat. Commun. **6**, 5913 (2015).
13. V. Studer, J. Bobin, M. Chahid, H. S. Mousavi, E. Candes, and M. Dahan, Proc. Natl. Acad. Sci. U.S.A **109**, E1679 (2012).
14. N. Radwell, K. J. Mitchell, G. M. Gibson, M. P. Edgar, R. Bowman, and M. J. Padgett, Optica **1**, 285 (2014).
15. R. W. Boyd and C. H. Townes, Appl. Phys. Lett. **31**, 440 (1977).
16. J. S. Dam, C. Pedersen, and P. Tidemand-Lichtenberg, Opt. Lett. **35**, 3796 (2010).
17. K. Huang, X. Gu, H. Pan, E. Wu, and H. Zeng, Appl. Phys. Lett. **100**, 151102 (2012).
18. G. B. Lemos, V. Borish, G. D. Cole, S. Ramelow, R. Lapkiewicz, and A. Zeilinger, Nature **512**, 409 (2014).
19. A. Tosi, D. A. Frera, A. B. Shehata, and C. Scarcella, Rev. Sci. Instrum. **83**, 013104 (2012).
20. Princeton Instruments, http://www.princetoninstruments.com/Uploads/Princeton/Documents/Datasheets/Princeton_Instruments_NIRvana_640_LN_revN1_8-4-15.pdf.
21. The data used to produce the content of this manuscript is available at http://dx.doi.org/10.5525/gla.researchdata.229.

optica

Photon-sparse microscopy: visible light imaging using infrared illumination : supplementary material

REUBEN S. ASPDEN,[1] NATHAN R. GEMMELL,[2] PETER A. MORRIS,[1] DANIEL S. TASCA,[1†] LENA MERTENS,[1] MICHAEL G. TANNER,[3‡] ROBERT A. KIRKWOOD,[3] ALESSANDRO RUGGERI,[4] ALBERTO TOSI,[4] ROBERT W. BOYD,[5,6] GERALD S. BULLER,[2] ROBERT H. HADFIELD,[3] AND MILES J. PADGETT[1,*]

[1] *School of Physics and Astronomy, University of Glasgow, G12 8QQ, UK*
[2] *School of Engineering & Physical Sciences, Heriot-Watt University, EH14 4AS, UK*
[3] *School of Engineering, University of Glasgow, G12 8QQ, UK*
[4] *Dipartimento di Elettronica, Informazione e Bioingegneria Politecnico di Milano, Piazza Leonardo da Vinci 32, 20133 Milano, Italy*
[5] *Department of Physics, University of Ottawa, Ottawa, Ontario, Canada*
[6] *The Institute of Optics and Department of Physics and Astronomy, University of Rochester, Rochester, NY 14627, USA*
† *Current address: Instituto de Física, Universidade Federal do Rio de Janeiro, Caixa-Postal 68528, Rio de Janeiro, RJ 21941-972, Brazil*
‡ *Current address: School of Engineering & Physical Sciences, Heriot-Watt University, EH14 4AS, UK*
*Corresponding author: miles.padgett@glasgow.ac.uk

Published 10 December 2015

This document provides supplementary information to "Photon-sparse microscopy: visible light imaging using infrared illumination," http://dx.doi.org/10.1364/optica.2.001049. We describe the optical configuration of the full imaging system and measure the resolution of the acquired images. The theoretical resolution of the imaging system is calculated, and we discuss the main experimental factors affecting the resolution of the imaging system. We present a method of photon counting within each frame of the acquired image, and use the statistical properties of the images to reconstruct images using far fewer photons than required to develop a conventional image. **© 2015 Optical Society of America**

http://dx.doi.org/10.1364/optica.2.001049.s001

Optical configuration of imaging system

The full schematic of our experiment is shown in Figure S1. Our down-conversion source consists a pulsed (100 MHz repetition rate, 10 ps pulse duration) solid-state pump laser operating at 355 nm with an average output power of 100 mW. The beam from this laser is collimated to a size of 470 μm FWHM and is then incident upon a 1 mm long ß-barium borate (BBO) crystal. The crystal is cut for type-I phase matching such that the beams of down-converted signal and idler photons are at 460 nm and 1550 nm, respectively. These photons are separated from each other using a dichroic beam splitter into two spatially distinct free-space optical paths where they are selected using high transmission interference filters. The idler path reimages the plane of the crystal to the object plane with a magnification of M=-1/2. Any photon transmitted by the object is reimaged to the plane of the SPAD with a further magnification of M=-10. The detection area of the SPAD is circular with a diameter of 25 μm, setting the width of the field of view of our imaging system to 250 μm. In the signal path, the plane of the crystal is reimaged to a time-gated, intensified CCD camera (ICCD), with a magnification of M=5. Thus the effective magnification through both arms of the imaging system from object to ICCD is M=-10.

The detection of an infrared photon is used to trigger the gate of the intensified camera such that the blue photon imaged on the camera and the infrared photon detected at the InGaAs/InP SPAD are from the same signal and idler photon pair. The combined response time from the input to the SPAD to the triggering of the intensifier in the ICCD (including the SPAD and the ICCD trigger

mechanism) is approximately 75 ns. Therefore, to ensure synchronization between signal and idler photons the signal arm is extended in length using a double-pass, image-preserving delay line comprising lenses and fold mirrors. The delay line is 25.2 m in length. We use a polarizing beam splitter (PBS) to allow entry into the double-pass section of the delay line and rotate the polarization through 90º within the delay line in order to reflect at the PBS on the return leg. The photon is then reimaged through a further telescopic imaging system before being detected by the camera.

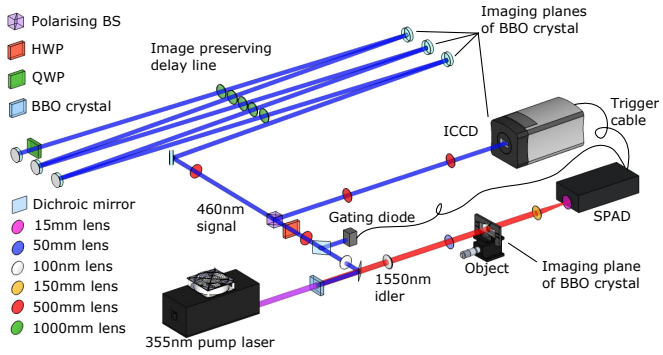

Figure S1. Full schematic of the experimental setup. The plane of the crystal is reimaged through the delay line to the ICCD camera in the signal path, and to the object plane in the idler path.

Measured Resolution

We determined the point spread function (PSF) of our system by analyzing the transition between the gold background and silicon central square in the image of the 50 µm side-length squares presented in Figure S2. The deconvolution of this acquired transition with a step function reveals a measured Gaussian PSF at the object plane of $2\sigma_{PSF} \approx 15$ µm. By considering this PSF and the size of our object we calculate that our acquired images in Figure 3 contain approximately ≈17 resolvable pixels in each transverse direction. There are many factors that limit the resolution of a trans-spectral imaging system [1,2]. However, in our ghost imaging system the resolution is primarily determined by a combination of the strength of the position correlation between signal and idler photons and the fidelity of the imaging optics

Theoretical Image Resolution and Influence of Heralding Detector

In a conventional microscope the illumination can be either spatially coherent or incoherent, albeit giving rise to subtly different point spread functions. A further subtlety in the limiting resolution of our ghost imaging system is the strength of the spatial correlations between the signal and idler photons. The degree to which the measured position of the visible signal photon recorded by the ICCD camera corresponds to that of the idler probe photon is a function of the phase-matching within the SPDC process. The standard deviation of the strength of the position correlation between signal and idler photons as measured in an image plane of the crystal is $\sigma_x = M\sqrt{0.455\, L\lambda_p/2\pi}$ [3-5] where M is the magnification between the crystal and measurement plane, L is the length of the non linear crystal and a pump beam of wavelength λ_p, giving in the plane of our object a position correlation of $2\sigma_x = 5$ µm. The resolution of our ghost imaging system cannot exceed this value, but obviously can be further degraded by the fidelity of the relay optics between the object plane and the ICCD. We note that our observed resolution is indeed lower than this predicted value a fact we attribute to the significant complexity of our image preserving delay line.

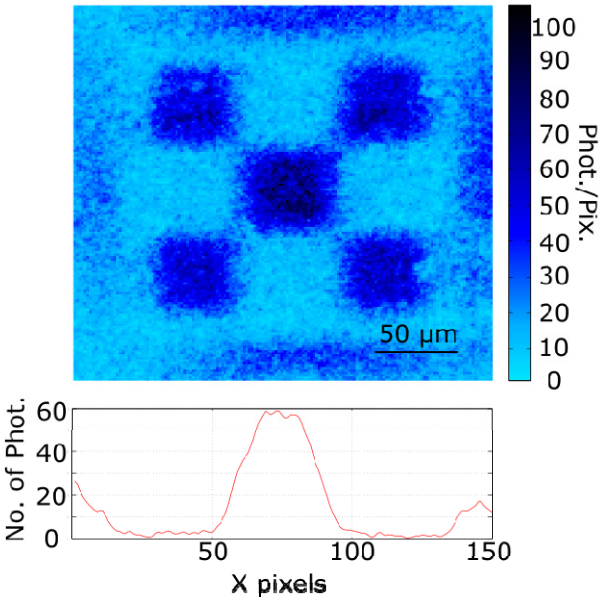

Figure S2. High contrast image of a five-spot test target. The deconvolution of the sharp transition between the edge of the gold background and silicon internal square and a step function was used to calculate the PSF, 2σPSF ≈15 µm, of our system. The cross section shown is the average of the rows across the middle square of the image.

Inherent in the strength of the position correlation is the divergence of the idler field, which places a limit upon the detection efficiency of the idler photon dependent upon the numerical aperture of the relay optics between the object plane and the single-pixel heralding detector. The calculated divergence of the idler in the plane of the object corresponds to a numerical aperture (NA) of 0.1 [6]. Given the magnification of the relay optics and 0.7 NA of the heralding detector we estimate the geometrical coupling efficiency of the idler to be of order 50%. Increasing this efficiency whilst maintaining the field of view of the system would require a heralding detector of increased area and/or numerical aperture. However, we note that our current detector represents the state of the art in term of both of these parameters

Image contrast

The contrast of the acquired images is a function of both the optical efficiencies in both optical arms, and the characteristics of the source and the heralding and imaging detectors. The heralding detector has an inherent dark count rate, and whilst these do not themselves appear in the image, these dark events gate the ICCD at a random time during which there is the possibility that it detects a photon from the down-conversion source that is not correlated with any image information. Consequently, the effect of dark counts is to create a background level, mapping the emission of the source, thereby limiting the image contrast.

The rate at which image photons are acquired depends upon the product of many efficiency factors covering the optical efficiency of both the infrared (see above) and visible relay optics, the quantum efficiency of both heralding and imaging detector and the rate at which the down-converted photons are generated. However, the pair generation rate cannot be arbitrarily increased. Fundamental to the operation of our approach is that the infrared and visible photons are spatially correlated. If multiple photon pairs are generated within the gate time of the ICCD camera then the spatial correlation between two detected photons is no longer guaranteed. Under conditions of multiple photon pairs, the

detected visible photons again map the emission profile of the source and may contain no image information. This limits the useful pair generation rate in accordance with the Poissonian statistics within the gate time of the camera. In our case we use a pair generation rate of approximately 10^6 photon pairs per second. In our experiment, we used a free-space coupled InGaAs/InP SPAD as the heralding detector. This has the advantage of a relatively large detector area (25 μm diameter) and high NA (~ 0.7), leading to a good detection efficiency of idler probe photons. Its main disadvantages are a high dark count rate (typically ~ 9,000 cps at 230 K when the detection efficiency is set to ~ 20%) and a maximum trigger rate limited by a necessary hold-off time between detections to avoid after-pulsing effects (which was typically set to 10 μs in these measurements, thus limiting the maximum count rate to $100\text{x}10^3$ counts per second (cps), well above the count rate of the idler photons in this experiment). However, the gated-mode operation was exploited to effectively reduce the rate of false idler detection by using a 1.4 ns duration gate synchronous with the source. Additionally, sine-wave gating of similar InGaAs/InP SPAD detectors have been shown to allow detection rates in excess of $100\text{x}10^6$ cps [7]. It is possible to use a single-photon sensitive detector based on superconducting nanowires (SNSPD) as a heralding detector [8]. However, current state of the art SNSPD detectors are mainly limited to single-mode collection and thus have a low NA and small detector diameter leading to a poor detection efficiency for idler probe photons of 1/N where N is the number of resolvable image pixels. Additionally, SNSPD operates at very low temperature (less than 4 K), thus requiring bulky cryogenic coolers.

However, latest generation of SNSPDs have near unity efficiency, coupled with low dark counts and deadtimes ~10 ns [9] and as such can acquire images more rapidly and with a potentially much higher image contrast. It is anticipated that multimode SNSPD's currently under development will enable a more efficient acquisition of higher contrast images.

Photon counting within each exposure of the camera

We are able to count the number of photons in the image by applying the following methodology [10]. During each firing of the intensifier, a charge is built up on each pixel, regardless of any signal present. We measure this by acquiring 100 dark images while blocking the input to the camera. Based on a histogram of these dark signals, a threshold signal value for each pixel is determined. When in imaging mode, a pixel signal greater than this threshold value is classified as a photon detection. We apply this threshold to each acquired frame and binarise the result. The number of photons in the image is the summation of these binary signals. The short gate time (10 ns) applied to our intensifier virtually eliminates any background counts. This elimination of the background combined with single-photon nature of our imaging system allows us to acquire images using a very small number of photons, i.e. with very low photon flux.

Image Reconstruction

To reconstruct the image from the raw data we follow the technique described in [11]. In essence, we minimise the total variation-squared of our image, subject to constraints imposed by the Poissonian nature of our data. We denote the measured photon number for each of the N image pixels to be ϕ_j and define the square of the total variation of the image as

$$R(\zeta_j) = \sum_{j=1}^{N} \left| \frac{d\zeta_j}{dx} \right|^2 + \left| \frac{d\zeta_j}{dy} \right|^2 \qquad \text{(S1)}$$

We also define a log likelihood function, L, of the reconstructed image as being

$$\ln L = \sum_{j=1}^{N} \phi_j \ln(\zeta_j + \varepsilon) - (\zeta_j + \varepsilon) - \ln(\phi_j !) \qquad \text{(S2)}$$

where ζ_j is the optimized data (as expressed in fractions of a photon) and ε is the average dark counts for each pixel.

The optimization of the reconstructed images is based upon iterative changes to the image to increase the merit function, which combines both the fit of the image to the data and its total variation-squared.

$$M = \ln L - \lambda R \qquad \text{(S3)}$$

λ is the weighting factor that sets a balance between a solution that satisfies the raw data and a solution that minimizes the total variation. Repeated iterative changes of pixel values within the image are performed and the image corresponding to a maximization of this merit function is found. If λ is set to zero then the optimized image corresponds exactly to the data recorded, whereas if λ is set to a very high value, the optimized image corresponds to a uniform level. In practice, the value of λ is set empirically or statistically at an intermediate value to give a reconstructed image, see Figure S3.

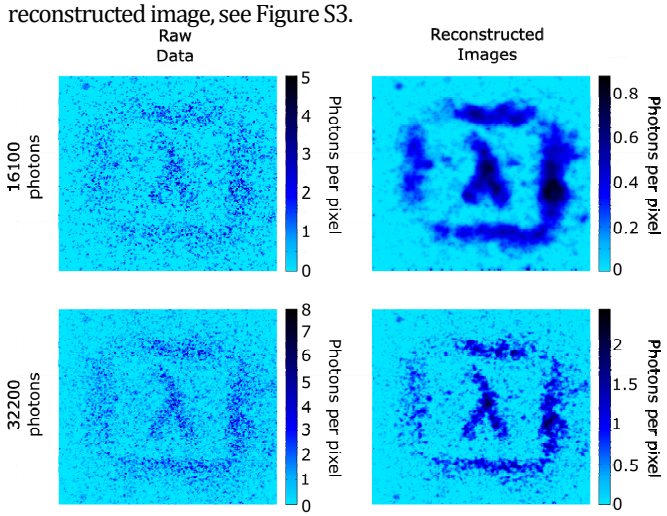

Figure S3. : Raw and reconstructed images. The images shown on the left hand side are the summation of 16100 and 32200 photons detected on the camera. We use optimisation techniques to reconstruct the images shown in the right hand column.

References

1. S. Karmakar, and Y. Shih, "Two-color ghost imaging with enhanced angular resolving power," Phys. Rev. A **81,** 033845 (2010).
2. M. H. Rubin, and Y. Shih, "Resolution of ghost imaging for nondegenerate spontaneous parametric down-conversion," Phys. Rev. A **78,** 7 (2008).
3. K. Chan, J. P. Torres, and J. H. Eberly, "Transverse entanglement migration in Hilbert space," Phys. Rev. A **75,** 050101 (2007).
4. M. P. Edgar, D. S. Tasca, F. Izdebski, R. E. Warburton, J. Leach, M. Agnew, G. S. Buller, R. W. Boyd and M. J. Padgett, "Imaging high-dimensional spatial entanglement with a camera," Nat. Commun. **3,** 984 (2012).
5. J. Schneeloch, and J. C. Howell, "Introduction to the Transverse Spatial Correlations in Spontaneous Parametric Down-Conversion through the Biphoton Birth Zone," arXiv:1502.06996v2 [quant-ph] (2015)

6. M. Padgett, "On the focussing of light, as limited by the uncertainty principle," J. Mod. Optic. **55,** 3083 (2008).
7. C. Scarcella, G. Boso, A. Ruggeri, and A. Tosi, "InGaAs/InP Single-Photon Detector Gated at 1.3 GHz With 1.5% Afterpulsing," Selected Topics in Quantum Electronics, IEEE J. **21,** 1 (2015).
8. C. M. Natarajan, M. G. Tanner, and R. H. Hadfield, "Superconducting nanowire single-photon detectors: physics and applications," Supercond. Sci. Technol. **25,** 063001 (2012).
9. F. Marsili, V. B. Verma, J. A. Stern, S. Harrington, A. E. Lita, T. Gerrits, I. Vayshenker, B. Baek, M. D. Shaw, R. P. Mirin, and S. W. Nam. "Detecting single infrared photons with 93% system efficiency". Nat Photonics **7,** 210 (2013).
10. D. S. Tasca, M. P. Edgar, F. Izdebski, G. S. Buller, and M. J. Padgett, "Optimizing the use of detector arrays for measuring intensity correlations of photon pairs," Phys Rev A **88,** 013816 (2013).
11. P. A. Morris, R. S. Aspden, J. E. C. Bell, R. W. Boyd, and M. J. Padgett, "Imaging with a small number of photons," Nat Commun **6,** 5913 (2015).